A resolution study for imaging and time reversal in random media

Liliana Borcea* George Papanicolaou† Chrysoula Tsogka‡

September 7, 2007

Abstract

We consider the inverse problem of array imaging of active sources (targets) in randomly inhomogeneous media, in a remote sensing regime with significant multiple scattering of the waves by the inhomogeneities. The active source emits a pulse that propagates through the inhomogeneous medium and is captured by an array of aperture a that is far from the source. We consider an analytical model for the matched field imaging functional and study the effect of random inhomogeneities on the resolution of the images produced. In our model the effect of the random medium is quantified by a single parameter, the narrow-band effective aperture of the array a_e. We give a robust procedure for estimating a_e, which is of great interest in many applications. In time reversal, knowing a_e allows us to estimate the refocused spot size, that is, the resolution of the time reversed, back-propagated field, which we can use in applications such as secure communications. The effective aperture a_e quantifies in an explicit way the loss of resolution in imaging active sources embedded at unknown locations in a randomly inhomogeneous medium, as well as the gain in resolution beyond the diffraction limit, the super-resolution, in time reversal.

1 Introduction

In many important applications, such as ultrasound medical imaging [18–20, 28], foliage penetrating radar [22, 34], land and shallow water mine detection [12], seismic inversion [5, 13], etc., one seeks to detect and image small or extended scatterers embedded in inhomogeneous media. We consider here randomly inhomogeneous media whose characterizing properties such as acoustic impedance, bulk modulus, etc. have a **known** large scale variation and an additional, **unknown**, weak, small scale variation, which we model as a random function of space. The scatterers are to be detected and imaged via an array of $2N + 1$ transducers (antennas), which can emit acoustic (electromagnetic) pulses and record the backscattered echoes. Depending on the application, there are several types of arrays. In ultrasound imaging, the arrays are usually linear, with $N \leq 100$, and the data recorded at the array, the response matrix $P(t) = (P_{pq}(t))$, can be measured and processed [20] efficiently. In seismic imaging the arrays can be very large but they are mostly passive, consisting of receivers and very few emitters [13]. In radar, the array may be fixed or it may be mounted on flying aircraft, thus generating a large synthetic aperture [15, 23, 29], etc. To fix ideas, let us suppose that we have a linear array of aperture a, that the targets are in the far field, at distance $L \gg a$, and that the

*Computational and Applied Math., MS 134, Rice University, Houston, TX 77005-1892.(borcea@caam.rice.edu)
†Department of Mathematics, Stanford University, Stanford, CA 94305. (papanico@math.stanford.edu)
‡CNRS/LMA, 31 Chemin Joseph Aiguier, 13402 Marseille cedex 20, FRANCE, (tsogka@lma.cnrs-mrs.fr)

response matrix $P(t)$ is measured for a sufficiently long time interval $(0, T]$ that contains all echoes from the targets.

Coherent array imaging of targets in known host media is well understood and there are several methods that work well. For example, we have: (a) Time domain, broad-band methods which use arrival time and/or amplitude information from the response matrix. This includes synthetic aperture radar (sonar) imaging [10, 12, 15, 23, 26] where only the diagonal part $P_{pp}(t)$ of the response matrix is recorded, and synthetic aperture radar interferometry [29], where a few diagonals of the response matrix are known. (b) Narrow-band methods, which use differential phase information from the response matrix and they image by beam forming [15, 23], by subspace methods such as MUltiple SIgnal Classification (MUSIC) [16, 24, 30, 33], or by least squares (maximum likelihood) direction of arrival methods [23, 32].

We are interested in imaging in randomly inhomogeneous media, in a regime where multipathing due to the inhomogeneities is significant. Such a regime arises in ultrasound imaging, underwater acoustics, ground or foliage penetrating radar, etc. and, depending on the applications, there is a variety of length scales that enter the formulation. For example, in underwater acoustics, the average wave propagation speed is $c_0 = 1.5$km/s, the central wavelength of the probing pulse may be $\lambda_0 \sim 1$m, the target range $L = 1 - 100$km, the propagation speed fluctuates by $1 - 2\%$ with correlation lengths $l_H \sim 100$m and $l_V \sim 10$m in the horizontal and vertical directions, respectively. In ultrasound imaging, $\lambda_0 \sim 1$mm, $c_0 = 1.5$km/s, $L \leq 10 - 50$cm, the fluctuations are around 1% with a correlation length $l \sim 1$mm, and so on. In spite of such a diversity of scales, we can roughly classify remote sensing problems in weakly fluctuating random media as belonging to either *high frequency* ($\lambda_0 \ll l \ll a \ll L$) or *radiative transport* ($\lambda_0 \sim l \ll a \ll L$) regimes. In both cases, even though the fluctuations in the medium are weak the waves travel over many correlation lengths and multipathing due to the inhomogeneities is significant. Imaging in regimes with significant multipathing is quite challenging and requires very different methods from the usual ones in a homogeneous or known environment. In particular, it requires understanding of wave propagation in random media.

There have been recently some theoretical and experimental developments in **time reversal**, where signals emitted by a source in the medium are recorded at the array, time reversed and sent back into the same medium. Because of the time reversibility of the wave equation we have (diffraction limited) refocusing of the time reversed signal at the source, in any non attenuating medium. For example, in a homogeneous medium we get a refocusing spot of approximate size $\lambda_0 L/a$, together with spurious Fresnel zones [11]. However, in random media, experimental [20, 25, 31] and theoretical [1, 6, 17, 27] studies show that the refocusing is much better and the Fresnel zones are eliminated. This is the phenomenon of **super-resolution** and it is due to the random inhomogeneities, which distribute the waves over a larger part of the medium than they would in the homogeneous case, and therefore carry more information about the source location. One can then say that the array appears to have an **effective aperture** $a_e \gg a$ and this leads to super-resolution and the elimination of Fresnel zones because of random phase cancellations. A quantitative assessment of super-resolution can be made, for example, by looking at the average, time reversed backpropagated field, calculated explicitly in [17]. However, it is remarkable that in appropriate regimes this phenomenon does not happen just in the mean but for almost all realizations of the random medium. This is the **self-averaging** phenomenon which has been explored numerically and analytically in [1, 6, 27], and for layered random media in [14, 21] and the references therein.

Since any reflection based imaging method involves some form of time reversal or backpropagation into the real (or a fictitious) medium, we can introduce statistically stable inversion methodologies for random media by taking advantage of our understanding of time reversal. In [4, 9] we developed such an approach to statistically stable imaging of small targets buried in a randomly inhomogeneous, isotropic, infinite medium. In this paper we study the resolution limit of images in such media. We consider a model for matched field imaging which accounts in a simple and explicit manner for the effect of the random medium on the image. This effect is quantified by a single parameter, the effective aperture a_e, which is unknown. We use our matched field model to estimate a_e and we demonstrate the feasibility of our approach with numerical simulations. In particular, we show that the estimated a_e predicts very accurately the spot size in time reversal in random media.

This paper is organized as follows. In section 2, we formulate the problem and the mathematical model. Time reversal in both deterministic and random media is discussed in section 3. Our results on matched field imaging in random media are given in section 4. In section 5 we use the matched field model derived in section 4 to estimate the effective aperture a_e, which depends on the random medium and on the range. We demonstrate the feasibility of the estimation process with numerical simulations in section 5.3. Finally, in section 6, we give a brief summary and conclusions.

2 Formulation and mathematical model

For simplicity we assume throughout the paper that there is a single target to be identified in the noisy medium. We distinguish between two types of targets: (1) Active ones, which emit a signal $f(t)$ that propagates through the medium and is received at the array and (2) passive ones, which are quiet and which can be detected from the scattered signals which have traveled from the emitting array elements to the target and back to the array. The target can be small, point like, or extended but of finite support. Imaging passive, small or extended targets in random media is considered in [8]. In this paper we focus attention on the case of a small, active target located at $\mathbf{y} = (0, 0, L)$ with respect to the center of the array, where L is the **range** and the **cross-range** is zero. The array contains point transducers located at $\mathbf{x}_p = (ph/2, 0, 0)$, for $p = -N, \ldots, N$. The separation $h/2$ between the array elements is chosen so that in a remote sensing regime the transducers behave like an array of **aperture** $a = Nh \ll L$ and not like separate entities, while interference is kept at a minimum. Often, $h = \lambda_0$, the wavelength of the carrier frequency of the pulse.

Suppose that we have an active target (source) which emits a pulse

$$f(t) = -\frac{d}{dt}\left(\frac{1}{\sqrt{2\pi\sigma_t^2}}e^{-i\omega_0 t}e^{-\frac{t^2}{2\sigma_t^2}}\right) = \frac{i\omega_0 + \frac{t}{\sigma_t^2}}{\sqrt{2\pi\sigma_t^2}}e^{-i\omega_0 t}e^{-\frac{t^2}{2\sigma_t^2}}, \tag{2.1}$$

where $\nu_0 = \omega_0/2\pi$ is the carrier frequency and $B = 1/(\sigma_t\nu_0)$ is the bandwidth of

$$\widehat{f}(\omega) = \int_{-\infty}^{\infty} f(t)e^{i\omega t}dt = i\omega e^{-\frac{\sigma_t^2(\omega-\omega_0)^2}{2}}. \tag{2.2}$$

Clearly, there are many choices for $f(t)$. For example, chirps such as $f(t) = e^{i\omega_0 t + i\alpha t^2}$ are commonly used in synthetic aperture radar imaging [10, 12, 15, 23, 26]. We take the pulse (2.1) just for

simplicity in the calculations. The signal received at $\mathbf{x}_p$ (see Figure 1) is

$$s_p(t) = f(t) \star G(\mathbf{x}_p, \mathbf{y}, t) = \frac{1}{2\pi} \int_{-\infty}^{\infty} \widehat{f}(\omega) \widehat{G}(\mathbf{x}_p, \mathbf{y}, t) e^{-i\omega t} d\omega, \tag{2.3}$$

where $\widehat{G}$ is the two point Green's function at radian frequency ω, and where $\star$ denotes convolution in time.

Figure 1: The setup for array time reversal and imaging

We choose the scalar wave equation as our mathematical model for wave propagation in the medium and we let $c(\mathbf{x})$ be the propagation speed at a point $\mathbf{x} \in \mathbb{R}^3$. This scalar model is appropriate for sonar and ultrasound regimes but not for electromagnetic waves or for seismic inversion, although it is often used there too. At frequency $\nu = \omega/2\pi$, the two point Green's function satisfies the reduced wave equation

$$\Delta \widehat{G}(\mathbf{x}, \mathbf{y}, \omega) + k^2 n^2(\mathbf{x}) \widehat{G}(\mathbf{x}, \mathbf{y}, \omega) = -\delta(\mathbf{x} - \mathbf{y}), \tag{2.4}$$

where $k = \omega/c_0$ is the wavenumber, c_0 is a reference speed of propagation and

$$n(\mathbf{x}) = \frac{c_0}{c(\mathbf{x})} \tag{2.5}$$

is the index of refraction of the medium. At infinity $\widehat{G}$ satisfies the radiation condition

$$\lim_{r \to \infty} r \left(\frac{\partial \widehat{G}}{\partial r} - ikn\widehat{G} \right) = 0, \tag{2.6}$$

where $r = |\mathbf{x} - \mathbf{y}|$.

Note that in this model we neglect the presence of boundaries and interfaces in the medium and focus attention just on the scattering by the random inhomogeneities. For simplicity we also neglect large scale background variations, although they can be accounted for easily in numerical calculations, and we let the fluctuations of the index of refraction be

$$\sigma \mu \left(\frac{\mathbf{x}}{l} \right) = n^2(\mathbf{x}) - 1, \tag{2.7}$$

where l is the correlation length (the scale at which the medium fluctuates), $\sigma \ll 1$ (weak fluctuations) and μ is a stationary, isotropic random field with mean zero and covariance

$$R(\mathbf{x}) = R(|\mathbf{x}|) = E\left\{\mu(\mathbf{x}' + \mathbf{x})\mu(\mathbf{x}')\right\}. \tag{2.8}$$

In **imaging**, we seek the unknown location $\mathbf{y}$ of the source that is buried in the unknown random medium by reversing in time the signals $s_p(t)$, $p = -N, ..., N$, and back-propagating them numerically into a **fictitious medium**, which is here homogeneous with constant sound speed c_0. This process, which is also referred to as migration [5, 13], or backprojection [26] in geophysics and in X-ray crystallography, respectively, is a form of **time reversal** [6, 14, 18–20, 25, 31]. In time reversal, the signals $s_p(t)$, $p = -N, ..., N$, received at the array, are time reversed and re-emitted into the **actual medium**. They back-propagate to the source and focus near it.

Thus, in both imaging and time reversal, we consider the back-propagated field at a "search" point $\mathbf{y}_s$ as shown in Figure 1. We take $\mathbf{y}_s$ in the plane determined by $\mathbf{y}$ and the array, at range $L + \eta$ and cross-range ξ. The **point-spread function** for time reversal is defined by

$$\Gamma^{TR}(\mathbf{y}, \mathbf{y}_s, t) = \frac{1}{2\pi}\int_{-\infty}^{\infty} e^{-i\omega t}\widehat{\Gamma}^{TR}(\mathbf{y}, \mathbf{y}_s, \omega)d\omega, \tag{2.9}$$

where

$$\widehat{\Gamma}^{TR}(\mathbf{y}, \mathbf{y}_s, \omega) = \overline{\widehat{f}(\omega)}\sum_{p=-N}^{N}\overline{\widehat{G}(\mathbf{x}_p, \mathbf{y}, \omega)}\widehat{G}(\mathbf{x}_p, \mathbf{y}_s, \omega), \tag{2.10}$$

and where the bar in (2.10) stands for complex conjugation. The point-spread function for imaging is given by

$$\Gamma^{IM}(\mathbf{y}, \mathbf{y}_s, t) = \frac{1}{2\pi}\int_{-\infty}^{\infty} e^{-i\omega t}\widehat{\Gamma}^{IM}(\mathbf{y}, \mathbf{y}_s, \omega)d\omega, \tag{2.11}$$

where

$$\widehat{\Gamma}^{IM}(\mathbf{y}, \mathbf{y}_s, \omega) = \overline{\widehat{f}(\omega)}\sum_{p=-N}^{N}\overline{\widehat{G}(\mathbf{x}_p, \mathbf{y}, \omega)}\widehat{G}_0(\mathbf{x}_p, \mathbf{y}_s, \omega) = \sum_{p=-N}^{N}\overline{\widehat{s}_p(\omega)}\widehat{G}_0(\mathbf{x}_p, \mathbf{y}_s, \omega), \tag{2.12}$$

and where $\widehat{G}_0(\mathbf{x}_p, \mathbf{y}_s, \omega)$ is the Green's function in a homogeneous medium

$$\widehat{G}_0(\mathbf{x}, \mathbf{y}, \omega) = \frac{e^{ik|\mathbf{x}-\mathbf{y}|}}{4\pi|\mathbf{x} - \mathbf{y}|}. \tag{2.13}$$

We note that Γ^{IM} differs from Γ^{TR} only insofar as the back-propagation is done in a homogeneous or reference medium in imaging.

In this paper, we analyze the point-spread functions for time reversal and imaging, both in the frequency and in the time domain, for randomly inhomogeneous media, in a remote sensing regime.

3 Time reversal

Because of the time reversibility of the wave equation, it is clear that if we capture waves at the array, time reverse them and send them back, they will focus near $\mathbf{y}$, the location of the source. The focusing is perfect if all the waves are captured by a time reversal mirror which encloses the

source. However, when only part of the waves are captured by an array of receivers/transmitters of aperture a, then the focusing resolution is diffraction limited and the point-spread function Γ^{TR} is not entirely concentrated at $\mathbf{y}$ but is spread out around it.

It is well known that the point-spread function for time reversal is tighter in random media than in homogeneous ones [6, 20]. This is due to multiple scattering (**multipathing**) in the random medium, which makes rays that are directed initially away from the array to be scattered onto it by the inhomogeneities. Thus, the random medium creates the illusion of a larger aperture and an improved refocusing resolution. This is the **super-resolution** phenomenon. It manifests itself by a smaller refocused spot and by the disappearance of the spurious Fresnel zones, because of random phase cancellations. Of course, multipathing has a negative effect on the captured signal as well, through the diminution of intensity carried away by rays scattered away from the array. However, the intensity loss can be compensated by amplification of the retransmitted signal, since the problem is linear.

In order to quantify the refocusing resolution in random media we use the **effective aperture**. We distinguish two types of effective apertures: (1) The narrow-band effective aperture a_e, determined by the random medium [6, 27] and the range, and (2) the broad-band effective aperture A_e, which depends on a_e and on the probing pulse $f(t)$, its bandwidth in particular. As shown in section 3.2, the effect of the random medium on the TR point-spread function Γ^{TR} is given explicitly by a_e and A_e, in the frequency and in time domain, respectively. Since the randomly scattering medium is not known, a_e is not known either, although, as we show in section 5, it can be accurately estimated.

Another remarkable property of time reversal, besides super resolution, is its deterministic nature, at least in the time domain, in a suitable remote sensing and multiple scattering regime [6, 27], where Γ^{TR} does not depend on the particular realization of the random medium, that is, it is **self-averaging**. In ultrasound and underwater sound experiments [20, 31] the statistical stability is a time domain phenomenon which does not apply to narrow-band signals. However, in high frequency regimes such as those occurring in optical or infrared applications, the time reversal point-spread function can be self-averaging even for narrow-band signals [27]. We focus attention on the lower frequency regimes with ordering of scales

$$\lambda_0 \sim l \ll a \ll L, \tag{3.1}$$

and we require that the signals be broad-band in order for Γ^{TR} to be self-averaging.

3.1 Time reversal in homogeneous media

The time reversal point-spread function in homogeneous media is

$$\Gamma_0^{\mathrm{TR}}(\mathbf{y}_s;t) = \frac{1}{2\pi}\int_{-\infty}^{\infty} \widehat{\Gamma}_0^{\mathrm{TR}}(\mathbf{y}_s;\omega)e^{-i\omega t}d\omega, \tag{3.2}$$

where

$$\widehat{\Gamma}_0^{\mathrm{TR}}(\mathbf{y}_s;\omega) = \overline{\widehat{f}(\omega)}\sum_{p=-N}^{N}\overline{\widehat{G}_0(\mathbf{x}_p,\mathbf{y};\omega)}\widehat{G}_0(\mathbf{x}_p,\mathbf{y}_s;\omega) = \overline{\widehat{f}(\omega)}\sum_{p=-N}^{N}\frac{e^{ik(|\mathbf{x}_p-\mathbf{y}_s|-|\mathbf{x}_p-\mathbf{y}|)}}{(4\pi)^2|\mathbf{x}_p-\mathbf{y}||\mathbf{x}_p-\mathbf{y}_s|}. \tag{3.3}$$

In a remote sensing regime ($a \ll L$), we can use the parabolic approximation of the phase

$$|\mathbf{x}_p-\mathbf{y}| = \left(L^2+x_p^2\right)^{\frac{1}{2}} \approx L + \frac{x_p^2}{2L}, \tag{3.4}$$

and, after some calculation [6, 7], we obtain

$$\Gamma_0^{\mathrm{TR}}(\xi,\eta;t) \approx -\frac{1}{2\pi}\int d\omega\, \frac{i\omega e^{-\frac{\sigma_t^2(\omega-\omega_0)^2}{2}}}{8\pi^2L^2h} e^{-i\omega\left[t-\frac{1}{c_0}\left(\eta+\frac{\xi^2}{2(L+\eta)}\right)\right]}\int_{-a/2}^{a/2} dx\, e^{-i\frac{\omega}{c_0}\left(\frac{\eta x^2}{2L(L+\eta)}+\frac{x\xi}{L+\eta}\right)}. \quad (3.5)$$

In particular, if we place a screen at the exact range ($\eta = 0$) and we observe the point-spread function for various cross ranges ξ, we have, after evaluating at the arrival time,

$$\Gamma_0^{\mathrm{TR}}(\xi,\eta=0;t=\frac{\xi^2}{2c_0L}) \approx \frac{c_0}{4\pi^2Lh\xi}\frac{-i}{\sqrt{2\pi\sigma_t^2}}\sin\left(\frac{\omega_0\xi a}{2c_0L}\right)e^{-\frac{a^2\xi^2}{8c_0^2L^2\sigma_t^2}}. \quad (3.6)$$

Thus, for pulse (2.1), the time reversal point-spread function in homogeneous media is determined by the product of sinc $\left(\frac{\pi\xi a}{\lambda_0 L}\right) = \sin\left(\frac{\pi\xi a}{\lambda_0 L}\right) / \left(\frac{\pi\xi a}{\lambda_0 L}\right)$ and a Gaussian $e^{-\frac{\xi^2}{2s^2}}$ with standard deviation

$$s = \frac{2c_0\sigma_t L}{a} = 2\nu_0\sigma_t\frac{\lambda_0 L}{a} = \frac{2}{B}\frac{\lambda_0 L}{a} \quad (3.7)$$

where $\omega_0 = 2\pi\nu_0$ and $B = 1/(\nu_0\sigma_t)$ is the bandwidth, $0 < B < 1$. For a narrow-band pulse s is large, the deterministic resolution limit $\frac{\lambda_0 L}{a}$ comes from the sinc function and the Fresnel zones are visible. For a broad-band pulse s is comparable to $\lambda_0 L/a$, which is the spot size determined by the Gaussian factor and the Fresnel zones are now eliminated. In either case, the larger the aperture a is the better the focusing.

3.2 Time reversal in random media

The time reversed, back-propagated field in the random medium is

$$\Gamma^{\mathrm{TR}}(\mathbf{y}_s,t) = \frac{1}{2\pi}\int \widehat{\Gamma}^{\mathrm{TR}}(\mathbf{y}_s;\omega)e^{-i\omega t}d\omega, \text{ for } \widehat{\Gamma}^{\mathrm{TR}}(\mathbf{y}_s;\omega) = \overline{\widehat{f}(\omega)}\sum_{p=-N}^{N}\left\langle\overline{\widehat{G}(\mathbf{x}_p,\mathbf{y};\omega)}\widehat{G}(\mathbf{x}_p,\mathbf{y}_s;\omega)\right\rangle, \quad (3.8)$$

where $\widehat{G}$ is the random, time harmonic Green's function and where, because of the self-averaging property of $\Gamma^{\mathrm{TR}}(\mathbf{y}_s,t)$ (see [6, 7, 27]), we can take the expectation of $\overline{\widehat{G}}\widehat{G}$. Then, using the moment formula [6, 7, 27]

$$\left\langle\overline{\widehat{G}(\mathbf{x}_p,\mathbf{y};\omega)}\widehat{G}(\mathbf{x}_p,\mathbf{y}_s;\omega)\right\rangle \approx \overline{\widehat{G}_0(\mathbf{x}_p,\mathbf{y};\omega)}\widehat{G}_0(\mathbf{x}_p,\mathbf{y}_s;\omega)e^{-\frac{k^2\xi^2a_e^2}{2L^2}}, \quad (3.9)$$

where $a_e = a_e(L) = \sqrt{DL^3}$ is a length that defines the effective aperture and D is a reciprocal length parameter that depends on the statistics of the random fluctuations of the speed of propagation. We then have [6, 7]

$$\begin{aligned}\widehat{\Gamma}^{\mathrm{TR}}(\mathbf{y}_s;\omega) &\approx \overline{\widehat{f}(\omega)}e^{-\frac{k^2\xi^2a_e^2}{2L^2}}\sum_{p=-N}^{N}\overline{\widehat{G}_0(\mathbf{x}_p,\mathbf{y};\omega)}\widehat{G}_0(\mathbf{x}_p,\mathbf{y}_s;\omega) = \widehat{\Gamma}_0^{\mathrm{TR}}(\mathbf{y}_s;\omega)e^{-\frac{k^2\xi^2a_e^2}{2L^2}} \\ &\approx e^{ik(\eta+\frac{\xi^2}{2(L+\eta)})}\frac{\overline{\widehat{f}(\omega)}}{8\pi^2L^2h}\int_{-a/2}^{a/2}e^{-ik\left(\frac{\eta x^2}{2L(L+\eta)}+\frac{x\xi}{L+\eta}\right)-\frac{k^2\xi^2a_e^2}{2L^2}}dx\end{aligned} \quad (3.10)$$

and, as in the homogeneous medium, we evaluate the point-spread function at the exact range ($\eta = 0$) and for a ξ which is smaller than the focal spot

$$\xi < \frac{\sigma_t c_0 L}{a_e} = \frac{\omega_0 \sigma_t}{2\pi} \frac{\lambda_0 L}{a_e}, \tag{3.11}$$

to obtain (see [6, 7])

$$\Gamma^{\rm TR}(\xi, 0; \frac{\xi^2}{2c_0 L}) \approx \frac{c_0}{4\pi^2 L h \xi} \frac{-i}{\sqrt{2\pi\sigma_t^2}} \sin\left(\frac{\omega_0 \xi a}{2c_0 L}\right) e^{-\frac{A_e^2 \xi^2}{8c_0^2 L^2 \sigma_t^2}} = \Gamma_0^{\rm TR}\left(\xi, 0; \frac{\xi^2}{2c_0 L}\right) e^{-\frac{2\pi^2 a_e^2}{L^2 \lambda_0^2}\xi^2}. \tag{3.12}$$

Here A_e is the broad-band effective aperture given by

$$A_e^2 = a^2 + 4\omega_0^2 \sigma_t^2 a_e^2 = a^2 + \left(\frac{4\pi a_e}{B}\right)^2. \tag{3.13}$$

Comparing this result with the deterministic one (3.6) we note that the physical array aperture a is replaced by a larger aperture ($A_e > a$) in random media, which explains the super-resolution phenomenon. The narrow-band effective aperture $a_e(L)$ can be very large in a regime with significant multipathing by inhomogeneities. In such a regime, the physical aperture a is negligible and there is remarkable focusing of $\Gamma^{\rm TR}$ on the source, even when the signal has been captured and time reversed by a small array. In the numerical simulations the range L is limited by our computational capabilities so a_e is roughly the same as a and the physical aperture still plays a role. The broad-band effective aperture A_e depends also on the bandwidth $B = 1/(\nu_0 \sigma_t)$, $0 < B < 1$, of the pulse. The smaller the bandwidth, the better the focusing. However, the bandwidth cannot be too small, since then statistical stability is lost. The precise trade-off between enhanced time-domain spatial focusing and loss of statistical stability with reduced bandwidth is not known. If $\Delta\omega$ is an estimate of the decoherence frequency interval for $\widehat{\Gamma}^{TR}$, then a good empirical rule for statistical stability in the time domain is that the bandwidth B divided by $\Delta\omega$ be large ($\sim 30 - 50$).

4 Matched field imaging

While the time reversal and imaging point-spread functions are the same in homogeneous (or deterministic) media, they behave very differently in random media. First, unlike Γ^{TR}, Γ^{IM} is wider in random media than in homogeneous ones, because multiple scattering impedes the identification of the source location. Second, the imaging point-spread function is not self-averaging. However, the time autocorrelation of Γ^{IM} is self-averaging. At zero time-lag this is the matched field imaging functional

$$\Gamma^{MF}(\mathbf{y}_s) = \int_{-\infty}^{\infty} |\widehat{\Gamma}^{IM}(\mathbf{y}, \mathbf{y}_s, \omega)|^2 d\omega, \tag{4.1}$$

which is statistically stable, and provides an estimate of the cross-range of the source. The range is lost, however, and it must be estimated separately, say from arrival time information. Various functionals for imaging the location of an active source and their relative performance are considered in [4, 9]. Our main result in this paper (see also [7]) is an analytical formula for the matched field functional $\Gamma^{MF}(\mathbf{y}_s)$ that can be used to estimate the narrow-band effective aperture a_e, when the range L is known.

The estimation of the effective aperture a_e is important not only in assessing quantitatively super-resolution in time reversal. As we show in section 4.2, a_e also quantifies the loss of cross-range resolution in matched field imaging.

4.1 Matched field in homogeneous media

In homogeneous media, the matched field estimator is

$$\begin{aligned}\Gamma_0^{\mathrm{MF}}(\xi,\eta) &= \frac{1}{2\pi}\int d\omega \left|\widehat{\Gamma}_0^{\mathrm{TR}}(\xi,\eta;\omega)\right|^2 \\ &\approx \frac{1}{2\pi}\int d\omega \left(\frac{\omega}{8\pi^2 L^2 h}\right)^2 e^{-\sigma_t^2(\omega-\omega_0)^2}\left|\int_{-a/2}^{a/2} dx\, e^{-i\frac{\omega}{c_0}\left(\frac{\eta x^2}{2L(L+\eta)}+\frac{x\xi}{L+\eta}\right)}\right|^2 . \end{aligned} \tag{4.2}$$

A contour plot is shown the left in Figure 2, for the parameters used in our simulations. Because this functional is an autocorrelation, range information is lost but the cross-range can be estimated. The cross-range resolution limit decreases as we search deeper in range (i.e. for large η) and it improves as we increase the array aperture. To illustrate this we evaluate (4.2) at the exact range ($\eta = 0$),

$$\Gamma_0^{\mathrm{MF}}(\xi,0) \approx \frac{c_0^2}{64\pi^4 L^2 h^2\sqrt{\pi\sigma_t^2}}\left[\frac{1-e^{-\frac{a^2\xi^2}{4c_0^2L^2\sigma_t^2}}}{\xi^2}+2\frac{\sin^2\left(\frac{\omega_0\xi a}{2c_0L}\right)}{\xi^2}e^{-\frac{a^2\xi^2}{4c_0^2L^2\sigma_t^2}}\right]. \tag{4.3}$$

We note now that, as in time reversal, the cross-range resolution of the matched field estimator is

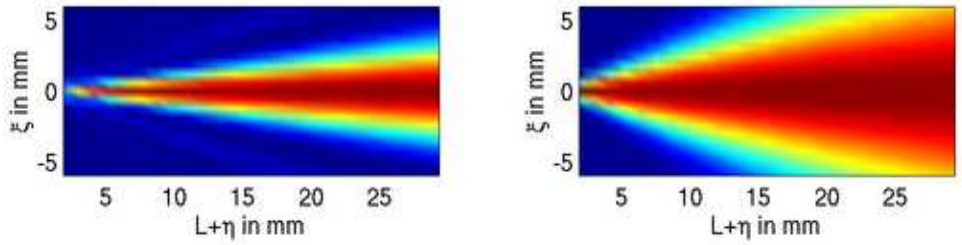

Figure 2: The matched field estimator in deterministic media (left figure, equation (4.3)) and in random media (right figure, equation (4.6)), for an effective aperture $a_e = 2a$.

inversely proportional to the aperture a. The larger a is, the better the accuracy of the estimated cross-range of the source. In the next section, we show that in random media matched field and time reversal behave very differently and that the physical aperture of the array is less important. In particular, we show that because of multiple scattering by the inhomogeneities the images are blurred in a manner quantified by the narrow-band effective aperture a_e.

4.2 Matched field in random media

The matched field in random media is very different from the time reversal process because the back-propagation is done numerically through a known, reference (homogeneous in our case) medium. The matched field functional is now

$$\widehat{\Gamma}^{\mathrm{MF}}(\mathbf{y}_S;\omega) = \left|\widehat{f}(\omega)\right|^2 \sum_{p=-N}^{N}\sum_{q=-N}^{N}\left\langle \overline{\widehat{G}_0(\mathbf{x}_p,\mathbf{y}_s;\omega)}G(\mathbf{x}_p,\mathbf{y};\omega)\overline{\widehat{G}(\mathbf{x}_q,\mathbf{y};\omega)}G_0(\mathbf{x}_q,\mathbf{y}_s;\omega)\right\rangle . \tag{4.4}$$

Because of its statistical stability in the time domain (see [6, 7, 27]), $\int d\omega \widehat{\Gamma}^{\mathrm{MF}}(\mathbf{y}_S;\omega)$ is essentially equal to its expectation. Using the moment formula [6, 7, 27]

$$\left\langle \overline{\widehat{G}(\mathbf{x}_p,\mathbf{y};\omega)}\widehat{G}(\mathbf{x}_q,\mathbf{y};\omega)\right\rangle \approx \overline{\widehat{G}_0(\mathbf{x}_p,\mathbf{y};\omega)}\widehat{G}_0(\mathbf{x}_q,\mathbf{y};\omega)e^{-\frac{k^2a_e^2}{2L^2}|\mathbf{x}_p-\mathbf{x}_q|^2}, \tag{4.5}$$

we find after some calculations given in [7] that

$$\Gamma^{MF}(\xi,\eta) \approx \tilde{C}(L,a)e^{-\frac{\xi^2}{2(L+\eta)^2}\left(\frac{L}{a_e}\right)^2}, \tag{4.6}$$

where $C(L,a)$ is independent of the random medium and of the cross-range ξ.

We have now a simple analytical expression that allows us to assess the effect of the random medium on imaging of the source by a matched field functional. Unlike time reversal, where a larger a_e (i.e. stronger multipath) gives a tighter point-spread function (see equation (3.12)), in imaging, the resolution is worse with larger a_e. Rich scattering environments produce blurry images.

5 Estimation of the effective aperture

Given the simple analytical expression for the matched field functional, in this section we estimate a_e by matching the formula (4.6) with the numerically calculated imaging functional $\Gamma_n^{MF}(\xi,\eta)$. First we describe the numerical simulations and the numerical procedure for estimating a_e. Then we demonstrate the feasibility of the estimation with numerical tests.

5.1 Setup for the numerical simulations

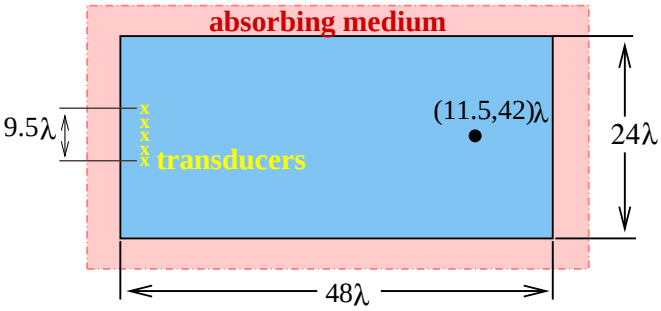

Figure 3: The computational setup. The dimensions of the problem are given in terms of the central wavelength $\lambda = 0.5$mm. The medium is considered to be infinite in all directions so in the numerical computations an absorbing layer surrounds the domain.

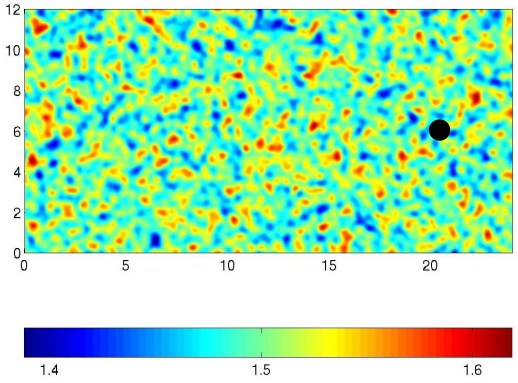

Figure 4: Typical realization of random sound speed $c(\mathbf{x})$. The target is shown as a large black dot ●. The units in the horizontal and vertical axes are mm and, in the color bar, km/s. The standard deviation for this example is $s = 4.95\%$

In the numerical simulations we generate the field $c(\mathbf{x})$ by a random Fourier series with mean $c_0 = 1.5$km/s, a Gaussian correlation function with correlation length $l = 0.3$mm and a standard

deviation ranging from 1% to 5%. A typical realization of the random medium is shown on the right in Figure 4. The width of the probing pulse (2.1) is $\sigma_t = 0.2325\mu$s, the central frequency is $2\pi\omega_0 = 3$MHz (i.e. $\lambda_0 = 0.5$mm) and the bandwidth is $2 - 4$MHz (measured at 6dB). We take an array of 10 transducers at a distance $h = \lambda_0/2$ from each other so the aperture is $a = 2.5$mm. The source is at range $L = 2$cm and at zero cross-range, measured with respect to the center of the array. To calculate the acoustic pressure at the array we solve the wave equation in the time domain with a finite element method that discretizes the mixed velocity-pressure (first order system) formulation [2, 3]. To simulate the infinite medium we surround the computational domain by a perfectly matched absorbing layer, as shown on the left in Figure 4. To avoid excessive computational cost we solve numerically the two dimensional problem, while all the analysis is based on three dimensional Green's functions. However, we have seen in the previous sections that it is the phase of the Green's function and not its amplitude that matters in imaging and time reversal, especially in the remote sensing regime. In this regime the phases of the Green's functions are the same in two and in three dimensions so we expect that the results of our direct numerical computations will be in good agreement with the theory.

5.2 The estimation of a_e

We estimate a_e by matching (4.6) with the numerically computed function $\Gamma_n^{MF}(\xi, \eta)$ as follows. With the simulation setup described in section 5.1 we solve the wave equation in the time domain, with an approximate point source located at $\mathbf{y} = (0, 0, L)$ and supported in a square element of size $\lambda_0/30$. At time $t = 0$, the source emits the pulse (2.1) and we calculate numerically the signals $s_p(t)$ received at the array elements $p = -N, \ldots, N$, for a time interval of length T, which is long enough to ensure that all is quiet for $t > T$. The numerical matched field functional at search point $\mathbf{y}_s = (\xi, 0, L + \eta)$ is then

$$\Gamma_n^{MF}(\xi, \eta) = \int \widehat{\Gamma_n^{MF}}(\xi, \eta, \omega) d\omega, \text{ where } \widehat{\Gamma_n^{MF}}(\xi, \eta, \omega) = \left| \sum_{p=1}^{N} \overline{\widehat{s_p}(\omega)} \widehat{G}_0(\mathbf{x}_p, \mathbf{y}_s, \omega) \right|^2 . \tag{5.1}$$

To find a_e we sample the search domain in steps of $\lambda_0/2$, we assume that we know the range L of the source, and we minimize the discrepancy between the theoretical and numerical matched field functionals (4.6) and (5.1), respectively,

$$\min_{\beta} \sum_{j=-5}^{5} \sum_{m=-4}^{4} \left[\gamma\left(j\frac{\lambda_0}{2}, m\frac{\lambda_0}{2} \right) - e^{-\frac{\beta(j\lambda_0/2)^2}{2(L+m\lambda_0/2)^2}} \right]^2 . \tag{5.2}$$

Here

$$\beta^2 = \frac{L}{a_e}, \tag{5.3}$$

and for each η we normalize (5.1) by

$$\gamma(\xi, \eta) = \Gamma_n^{MF}(\xi, \eta) / \max_{\xi} \Gamma_n^{MF}(\xi, \eta). \tag{5.4}$$

The minimization (5.2) is done in MATLAB with *fminunc*.

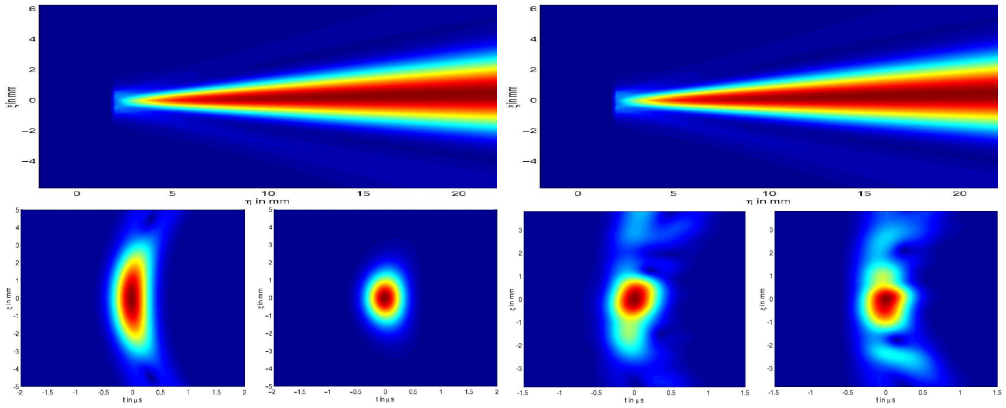

Figure 5: Top: $\Gamma^{\mathrm{MF}}(\mathbf{y}_s)$ computed numerically for two realizations of the random medium, the estimation of a_e is 1.43mm (resp. 1.47mm) for the data on the left (resp. right). The horizontal axis is $L + \eta$ in mm and the vertical axis is the cross-range ξ in mm. Bottom (left to right): the theoretical prediction of the time reversed field in a homogeneous medium, in a random medium (obtained using $a_e = 1.45$mm in (3.12)) and the numerically calculated time reversed field for the same two realizations of the random medium considered in the top matched field estimates. The horizontal axis is time in μs and the vertical axis is the cross-range ξ in mm.

5.3 Estimation results

The estimated values of a_e are 1.43, 1.54, 1.37, 1.46 in mm, for four realizations of the random medium. We show in the top two panels of Figure 5 the numerically computed matched field functional (5.1), for two such realizations. The theoretical matched field functional (4.6) when calculated with the estimated a_e looks the same as the numerical ones. In order to assess the feasibility of our approach we use the estimated a_e in the expression of the theoretical time reversal point-spread function (3.12), and we compare the result with the numerically simulated time reversed field. The results are shown in the bottom panels of Figure 5. First, we observe the super-resolution phenomenon, because the point-spread function is tighter in a random medium than in the homogeneous one. Second, we note that the theoretical model (3.12) with the estimated a_e gives a rather accurate spot size at the source. The fluctuations that we observe (for large ξ)in the numerically computed field (right bottom panels) are not captured by the theoretical model (3.12), as expected, but the refocused field is captured correctly near the source. Finally, the statistical stability of both (5.1) and the time reversed field is observed in numerical simulations with several realizations of the random medium.

6 Summary

We have analyzed matched field imaging of small, active sources at unknown locations in a random medium, in a remote sensing regime with significant multipathing of the waves scattered by the inhomogeneities. We have shown that the imaging resolution in random media can be quantified by a single parameter, the narrow-band effective aperture a_e. We have derived a simple analytical expression for the matched field imaging functional which can be used for estimating the unknown

a_e in a robust way. We have assessed the feasibility of our estimation approach with direct numerical simulations. We have obtained remarkably good agreement between the estimated effective aperture and the observed refocused spot size in direct numerical simulations of time reversal.

Acknowledgments

The work of L. Borcea was partially supported by the Office of Naval Research, under grant N00014-02-1-0088. The work of G. Papanicolaou was supported by grants AFOSR F49620-01-1-0465 and ONR N00014-02-1-0088.

References

[1] G. Bal, G. C. Papanicolaou, and L. Ryzhik. Self-averaging in time reversal for the parabolic wave equation. *Stochastics and Dynamics*, 2:507–531, 2002.

[2] E. Bécache, P. Joly, and C. Tsogka. Etude d'un nouvel élément fini mixte permettant la condensation de masse. *C. R. Acad. Sci. Paris Sér. I Math.*, 324:1281–1286, 1997.

[3] E. Bécache, P. Joly, and C. Tsogka. An analysis of new mixed finite elements for the approximation of wave propagation problems. *SIAM J. Numer. Anal.*, 37:1053–1084, 2000.

[4] J. Berryman, L. Borcea, G. C. Papanicolaou, and C. Tsogka. Statistically stable ultrasonic imaging in random media. *Journal of Acoustical Society of America*, 112:1509–1522, 2002.

[5] N. Bleistein, J.K. Cohen, and J.W. Stockwell Jr. *Mathematics of multidimensional seismic imaging, migration, and inversion*. Springer, New York, 2001.

[6] P. Blomgren, G. Papanicolaou, and H. Zhao. Super-resolution in time-reversal acoustics. *Journal of the Acoustical Society of America*, 111:238–248, 2002.

[7] L. Borcea, G. C. Papanicolaou, and C. Tsogka. Estimation of the refocusing resolution for time reversal in scattering media. *SIAM Journal on Multiscale Modeling and Simulation, submited*, 2003.

[8] L. Borcea, G. C. Papanicolaou, and C. Tsogka. Imaging the reflectivity of extended scatterers in random media. *preprint*, 2003.

[9] L. Borcea, G. C. Papanicolaou, C. Tsogka, and J. Berryman. Imaging and time reversal in random media. *Inverse Problems*, 18:1247–1279, 2002.

[10] B. Borden. Mathematical problems in radar inverse scattering, topical review. *Inverse Problems*, 18:R1–R28, 2002.

[11] M. Born and E. Wolf. *Principles of optics*. Academic Press, New York, 1970.

[12] L. Carin, N. Geng, M. McClure, Y. Dong, Z. Liu, J. He, J. Sichina, M. Ressler, L. Nguyen, and A. Sullivan. Wide-area detection of land mines and unexploded ordnance. *Inverse Problems*, 18:575–609, 2002.

[13] J. F. Claerbout. *Fundamentals of geophysical data processing : with applications to petroleum prospecting*. CA : Blackwell Scientific Publications, Palo Alto, 1985.

[14] J.F. Clouet and J.P. Fouque. A time-reversal method for an acoustical pulse propagating in randomly layered media. *Wave Motion*, 25:361–368, 1997.

[15] J.C. Curlander and R.N. McDonough. *Synthetic Aperture Radar*. Wiley, New York, 1991.

[16] A.J. Devaney. Super-resolution processing of multi-static data using time reversal and MUSIC. *to appear in J. Acoust. Soc. Am.*, 2002.

[17] D. R. Dowling and D. R. Jackson. Narrow band performance of phase conjugate arrays in dynamic random media. *J. Acoust. Soc. Am.*, 91:3257–3277, 1992.

[18] M. Fink. Time reversal mirrors. *J. Phys. D*, 26:1330–1350, 1993.

[19] M. Fink. Time reversed acoustics. *Phys. Today*, 50:34–40, 1997.

[20] M. Fink and C. Prada. Acoustic time-reversal mirrors, topical review. *Inverse Problems*, 17:R1–R38, 2001.

[21] J. P. Fouque and K. Solna. Time-reversal aperture enhancement. *preprint*, 2000.

[22] A. Gustavsson, P. O. Frölind, H. Hellsten, T. Jonsson, B. Larsson, G. Stenström, and L. M. H Ulander. Development and operation of the foa carabas hf/vhf-sar system. In *Proc. 4th Int. Workshop on Radar Polarimetry*, Nantes, France, July 1998.

[23] S. Haykin, J. Litva, and T. J. Shepherd. *Radar Array Processing*. Springer-Verlag, New York, 1993.

[24] A. Kirsch. The music-algorithm and the factorization method in inverse scattering theory for inhomogeneous media. *Inverse Problems*, 18(4):1025–1040, 2002.

[25] W. A. Kuperman, W. S. Hodgkiss, H. C. Song, T. Akal, C. Ferla, and D. R. Jackson. Phase conjugation in the ocean : Experimental demonstration of an acoustic time reversal mirror. *J. Acoust. Soc. Am.*, 103:25–40, 1998.

[26] C. J. Nolan and M. Cheney. Synthetic aperture inversion. *Inverse Problems*, 18(1):221–235, 2002.

[27] G. Papanicolaou, L. Ryzhik, and K. Solna. Statistical stability in time reversal. *To appear in the SIAM J. Applied Mathematics*, 2003.

[28] C. Prada, S. Manneville, D. Spolianski, and M. Fink. Decomposition of the time reversal operator: Detection and selective focusing on two scatterers. *J. Acoust. Soc. Am.*, 99:2067–2076, 1996.

[29] P. A. Rosen, S. Henseley, I. R. Joughin, F. K. Li, S. N. Madsen, E. Rodriguez, and R. M. Goldstein. Synthetic aperture radar interferometry. *Proceedings of the IEEE*, 88(3):333–382, 2000.

[30] R. O. Schmidt. Multiple emitter location and signal parameter estimation. *IEEE Trans. Antennas Prop.*, AP-34:276–280, 1986.

[31] H. C. Song, W. A. Kuperman, and W. S. Hodgkiss. Iterative time reversal in the ocean. *J. Acoust. Soc. Am.*, 105:3176–3184, 1999.

[32] B.D. Steinberg. *Microwave Imaging with Large Antenna Arrays.* Wiley, New York, 1983.

[33] P. Stoica and R.L. Moses. *Introduction to Spectral Analysis.* Prentice Hall, New Jersey, 1997.

[34] L. M. H. Ulander and H. Hellsten. Low-frequency ultar-wideband array-antenna sar for stationary and moving target imaging. In *Conf. Proc. SPIE 13th Annual Int. Symp. on Aerosense*, Orlando, FL, April 1999.